Supplementary Information for

The role of the permanent wilting point in controlling the spatial distribution of precipitation

Cathy Hohenegger and Bjorn Stevens

Corresponding author: Cathy Hohenegger.
E-mail: cathy.hohenegger@mpimet.mpg.de

This PDF file includes:

Supporting Information Text

In this supporting information we investigate the generality of our results, first with respect to the derived theoretical model and the expected strengths of the underlying circulations, and second with respect to our modelling set-up.

1. Theoretical model

In the main text we combine the linearized version of the surface energy budget (Eq. 1) with a mixed layer model of a transiently growing boundary layer (Eqs. 2-3) and theory describing density current propagation (Eq. 4) to understand to which extent the soil needs to dry out to affect the radiatively driven circulation. In the following we first give some more details on the computation of the variables entering Eqs. (1-4). We then assess the validity of our theoretical model by using another approach based on an equilibrium boundary layer (1), before assessing the generality of the results by considering another simulation with a modified resistance formulation. Finally, we substantiate our claim that shutting down evaporation produces stronger circulations than radiative effects do by conducting supplementary sensitivity experiments.

To solve the linearized version of the surface energy budget (Eq. 1) we assume that the surface and atmospheric states are known in the limiting case of r_s approaching 0 s m^{-1}, i.e. in the precipitating region. From the simulation we get values of $Q = 380$ W m^{-2}, $\frac{\partial q_s}{\partial T} = 0.0015$ kg kg^{-1} K^{-1}, $q_s = 0.025$ kg kg^{-1} and $RH = 0.85$. All the values have been averaged over the precipitating area, as defined in Fig. 1 for each day, from 6 to 18 LT, and from days 25 to 150. We only consider daytime values as the implicit assumption that the averaged surface flux equals the average of its individual components breaks down when including the nighttime hours. The value for $F_{SH}(r_s = 0)$ is taken from the sensible heat flux values binned by soil moisture (see Fig. 4a), as averaged over the soil moisture classes 0.8 to 1. The value is 37.9 W m^{-2}. r_a is also not directly diagnosed from the simulation output because r_a can reach high values at specific grid points, which strongly biases the estimate of its mean. Instead, we choose r_a so as to match $F_{SH}(r_s = 0)$. This gives a value of 47 s m^{-1}, not too far from its simulated median value of 60 s m^{-1}.

To solve the boundary layer Eqs. 2-3 we correspondingly take values of: $t = 12$ h, $\Gamma = 4.5$ K km^{-1} and $\theta_v^0 = 297$ K. Whereas Γ is diagnosed from the simulation output by fitting a line to the profile of virtual potential temperature, we choose θ_v^0 so that the value of $\theta_v(r_s = 0)$ obtained from Eq. 2 is consistent with the above value of q_s.

Finally, in Eq. 4 describing the density current propagation, we assume for simplicity that the depth of the circulation H is constant with a value of 1000 m. The density current parameter k is set to 0.37. Different values of k have been reported in the literature, but generally k<1 (2, 3). We choose a value of $k = 0.37$ which gives best agreement between diagnosed and theoretically computed values of c.

The derivation and application of Eqs. 1-4 is based on various simplifications and assumptions. In particular, we view the boundary layer as transiently growing over the nonprecipitating region in response to the changing soil moisture conditions. We also do not include the radiative cooling in the boundary layer with the underlying motivation of separately quantifying the two forcings, radiative cooling and surface warming, in their ability to generate circulations. A contrasting approach to relate soil moisture to the propagation velocity of the soil moisture-induced circulation c would thus be to use an idealized equilibrium mixed layer of the boundary layer coupled to the land surface and including radiative cooling, as in (1). In this approach, we relate the soil moisture resistance to the boundary layer properties using Figs. 1a and 3a of (1) instead of our Eqs. (1-3).

Figure 1a of (1) allows us to relate the boundary layer thickness, expressed as p_{lcl}, to the soil moisture resistance r_s:

$$p_{lcl} = a + b \cdot r_s \qquad [S1]$$

with a intercept and b slope. Given the value of Γ in our simulation, we derive the intercept and slope by fitting a line to the curve for a stability of 0.05 K hPa^{-1} below a resistance value of 300 s m^{-1} (see Fig. S1a for typical resistance values associated with our resistance formulation). The obtained values are: $a = 45$ hPa and $b = 0.32$ hPa m s^{-1}. We then relate p_{lcl} to the potential temperature θ based on Fig. 3a of (1):

$$\theta = m + q \cdot p_{lcl} \qquad [S2]$$

with m intercept and q slope. The values are $m = 299.$ K and $q = 0.044$ K hPa^{-1} as approximated from Fig. 3a of (1), again for the curve with a stability of 0.05 K hPa^{-1}. The so derived θ values are used instead of θ_v to solve Eq. 4. The resulting c is plotted in Fig. S1b together with our previous theoretical estimate. The two curves show a similar behavior. They both exhibit a sharp increase of c close to the permanent wilting point and predict that a complete drying of the soil is needed to offset the radiatively driven circulation. Hence the details of the derivation do not seem to matter much, a finding that reflects the fact that the behavior of c is strongly dictated by the very non-linear behavior of the resistance function.

To further test to which extent the soil needs to dry out to affect the precipitation distribution, we alter the shape of the resistance function (see Eq. 5) by using a $r_{s,fc}$ of 50 s m^{-1} instead of 1 s m^{-1}. This corresponds to the value used by ECMWF in their land surface model for bare soil evaporation. The new simulation is restarted from a time in the standard experiment (here day 36) when the radiatively driven circulation had time to organize the convection, but before strong enough soil moisture gradients had time to develop (see also next section). Figure S2 is the pendant to Fig. 4. The values used to construct Fig. S2 are : $Q = 398$ W m^{-2}, $\frac{\partial q_s}{\partial T} = 0.0017$ kg kg^{-1} K^{-1}, $q_s = 0.027$ kg kg^{-1}, $RH = 0.76$ and $r_a = 69.7$ s m^{-1}. Since r_s never approaches 0 s m^{-1} in this simulation, we use instead of $F_{SH}(r_s = 0)$ the value of F_{SH} by a soil moisture of 1. The value is 44 W m^{-2}. Figure S2 indicates that, as in the standard experiment, the sensible heat flux and the theoretical velocity of the soil moisture-induced circulation c sharply increase close to the permanent wilting point. The theoretical estimate predicts a soil

moisture value of 0.20 needed to offset the radiatively driven circulation. From the simulation, the precipitation starts falling in the previously nonprecipitating region due to the soil moisture-induced circulation by a soil moisture value of 0.21. This is close to our theoretical estimate and confirms that a strong drying of the soil, down to less than 15% of its water availability, is needed to offset the radiatively driven circulation. Figure S2 also confirms the validity of our theoretical model to capture the simulated behavior. As an even more extreme (and slightly unrealistic) case, we conducted a simulation restarted with a $r_{s,fc}$ of 100 s m^{-1}. In this case, precipitation starts falling over the previously nonprecipitating area by a soil moisture of 0.24. This remains a significant drying with the soil water down to 30% of its availability.

Our theoretical analysis and simulation results emphasize that, at the latest by the permanent wilting point, the soil moisture-induced circulation becomes stronger than the radiatively driven circulation. We investigate whether there may nevertheless be cases where the soil moisture-induced circulation may not be able to reverse the radiatively driven circulation. To that aim we perform simulations with the UCLA-LES with no rotation, no radiation and fixed surface fluxes. We use a channel geometry with a domain of 240 km x 48 km x 5 km and a grid spacing of 100 m in the horizontal and 50 m in the vertical. To mimic the radiatively driven circulation, we split the domain into two halves (in the x-direction) and specify different cooling rates below 1 km on each half, as the radiatively driven circulation is due to cooling in the planetary boundary layer (as found in previous RCE experiments). To mimic the soil moisture-induced circulation, we specify two different values of the sensible heat flux on each half of the domain. The advantage of this set-up is that it allows us to easily control the strength of either the radiatively driven circulation or of the surface-induced circulation by altering the values of the cooling rates and/or of the surface fluxes. Note that the UCLA-LES is used here in its dry mode to avoid that the development of convection affects the characteristics of the circulation.

We compare a simulation with an anomalous sensible heat flux of 150 W m^{-2} on one of the patch, corresponding to the daily averaged net surface radiation in our simulation and hence upper limit on the possible surface warming, to simulations with anomalous cooling rates varying between -1 and -5 K day^{-1}. In every case, the circulation induced by the sensible heat flux difference is stronger than the radiatively driven circulation. As an extreme case we conduct one simulation with an unrealistically strong cooling rate of -10 K day^{-1} imposed on the left half of the domain. After the radiatively driven circulation has developed, we impose the sensible heat flux perturbation of 150 W m^{-2} on the left half of the domain. As illustrated in Fig. S3 the circulation reverses due to the sensible heat flux perturbation. From this we conclude that the soil moisture-induced circulation wins over the radiatively driven circulation, in agreement with the much stronger temperature perturbation generated in the former case.

2. Modeling set-up

In our study we use a simple representation of the land surface (see materials and methods) to investigate the effect on the precipitation distribution of a variable and possibly limited supply of moisture from the land surface to the atmosphere. Despite the simplicity of our representation, a few parameters describing the properties of the land surface need to be specified. Those are the heat capacity of the land surface, the soil depth, the initial soil moisture content as well as field capacity, permanent wilting point and soil moisture resistance at field capacity. We investigate in this section the robustness of our results with respect to such parameter choices.

We use a heat capacity of 20000 J K^{-1} m^{-2}, originally based on observations taken at Cabaw and employed in previous idealized studies on land-atmosphere interactions (4, 5). This choice results in a diurnal temperature range of 17 K, not too dissimilar from the 14 K obtained in the single column RCE study of (6) for their land-like set-up. The dependency of the self-aggregation of convection on the heat capacity was investigated in (7) for slab oceans and using fixed insolation. Having a diurnal cycle alters the response of the self-aggregation. On the one hand, small heat capacities favor a strong variability in surface temperature and a strong surface warming, which impedes the self-aggregation of convection as explained in (7). On the other hand, small heat capacities lead to a strong nighttime cooling, particularly in clear areas. This can enhance the boundary layer stability, make it more difficult to trigger deep convection on the next day and may result in the triggering of shallow convection instead of deep convection in the areas that were strongly cooled at night. Shallow clouds are crucial to spin-up the radiatively driven circulation that allows the convection to self-aggregate (8). How these two opposite effects balance depends non-linearly on the heat capacity. We vary the heat capacity from $2 \cdot 10^2$ to $2 \cdot 10^{10}$ J K^{-1} m^{-2}, incrementing it by factors of 10. As shown in Fig. S4, the nighttime cooling increases disproportionally compared to the surface warming as the heat capacity is reduced, a feature already noted in (9). As a result, only in the simulations with heat capacities of $2 \cdot 10^5$ J K^{-1} m^{-2} and $2 \cdot 10^6$ J K^{-1} m^{-2} the self-aggregation of convection is impeded, although it cannot be excluded that running the simulations for a longer time or on a bigger domain might eventually lead to self-aggregation. Note that if the diurnal cycle in insolation is removed, none of the simulations with heat capacity below $2 \cdot 10^6$ J K^{-1} m^{-2} self-aggregates, as expected from (7). Land surface models used in climate models employ skin layers with very small heat capacities, even neglecting it completely for non-vegetated surfaces. Hence, despite the order of magnitude difference in heat capacities between land and ocean, both tend to support the self-aggregation of convection, albeit in their own ways.

The effect of the chosen initial soil moisture and soil depth is straightforward. In the standard configuration, with an initial soil moisture of 0.475 and soil depth of 1 m, it takes more than ten days for the self-aggregation to start and fifty-four days for the first grid points to reach their permanent wilting point. Reducing the initial soil moisture or the soil depth allows the soil to more rapidly reach its permanent wilting point with a corresponding earlier homogenization of the precipitation distribution by the soil moisture-induced circulation.

The impacts of the remaining parameters, field capacity ϕ_{fc}, permanent wilting point ϕ_{pwp} and soil moisture resistance by

field capacity $r_{\text{s,fc}}$, may be best understood by considering their collective effect on the value of the soil moisture resistance r_{s} during the first simulation days. For values of r_{s} that are much smaller than the atmospheric resistance r_{a}, as in our standard configuration, the convection self-aggregates and remains self-aggregated until the soil moisture-induced circulation kicks in. Values of r_{s} in the order of r_{a} are accompanied by a stronger sensible heat flux and stronger surface warming. Although patches of clear air randomly develop, the expansion of which is instrumental to the self-aggregation of convection (7, 8), the underlying radiatively driven circulation is not strong enough to maintain them. The patches disappear within a day and the convection remains randomly distributed. As examples, increasing $r_{\text{s,fc}}$ from 1 to 50 s m^{-1} prevents the self-aggregation of convection, whereas using a $r_{\text{s,fc}}$ of 50 s m^{-1} combined with a ϕ_{fc} of 0.1 and a ϕ_{pwp} of 0.05, akin to a sand soil type instead of a loamy clay, allows the atmosphere to self-aggregate. This is consistent with the different magnitudes of r_{s} at initial time: 0.64 s m^{-1} in our standard experiment, 31.9 s m^{-1} for the case of $r_{\text{s,fc}} = 50$ s m^{-1} and 5.9 s m^{-1} for the sand soil type.

Independently of the values of ϕ_{fc}, ϕ_{pwp} and $r_{\text{s,fc}}$, a simulation that starts from a state in which the convection is already self-aggregated remains self-aggregated until the soil moisture-induced circulation sets in. This phenomenon of hysteresis regarding the self-aggregation of convection has already been documented in simulations using fixed SST (8). From this we conclude that interactive soil moisture always acts to disrupt the self-aggregation of convection. Although the occurrence of self-aggregation is dependent upon model details, the shutting down of evaporation over nonprecipitating region robustly acts to bring the precipitation to the nonprecipitating region.

**Cathy Hohenegger and Bjorn Stevens**
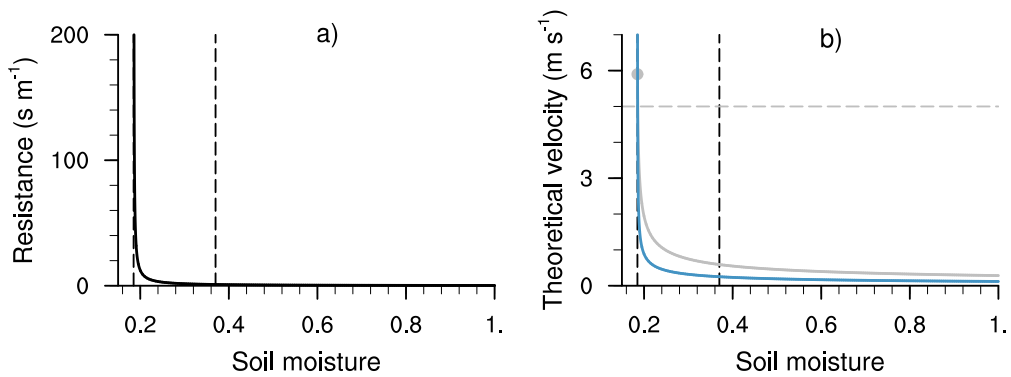
Fig. S1. (a) Soil moisture resistance and (b) theoretical value of the soil moisture-induced circulation velocity c as function of soil moisture. The grey curve uses a transiently growing boundary layer (as in Fig. 4b) and the blue curve is based on an equilibrium boundary layer after ([1]). The two dashed black lines indicate field capacity (0.37) and permanent wilting point (0.185). Circle symbol for the simulated soil moisture value one day before the precipitation starts falling in the nonprecipitating region.
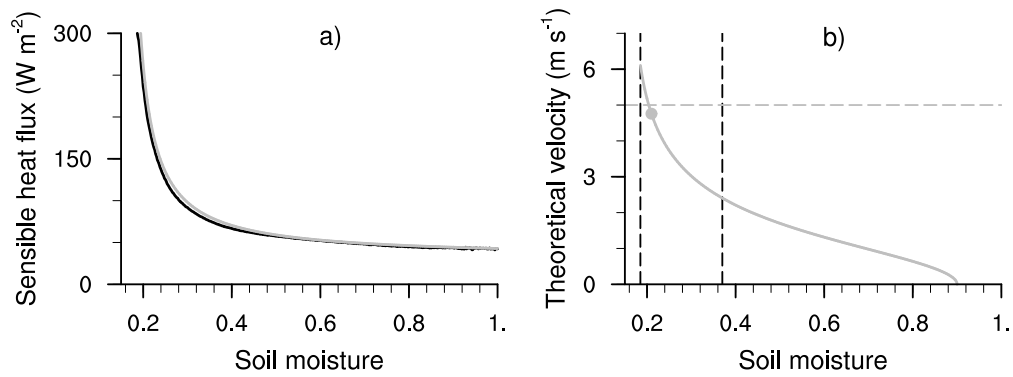
Fig. S2. (a) Daytime averaged values (6-18 LT) of sensible heat flux binned by soil moisture (black) together with their theoretical estimate (grey) as well as (b) theoretical velocity c of the soil moisture-induced circulation as function of soil moisture. The two dashed black lines are field capacity (0.37) and permanent wilting point (0.185). Circle symbol for the simulated soil moisture value one day before the precipitation starts falling in the nonprecipitating region. The simulation is restarted from our standard experiment on day 36 with a $r_{s,fc}$ of 50 s m^{-1} instead of 1 s m^{-1}.
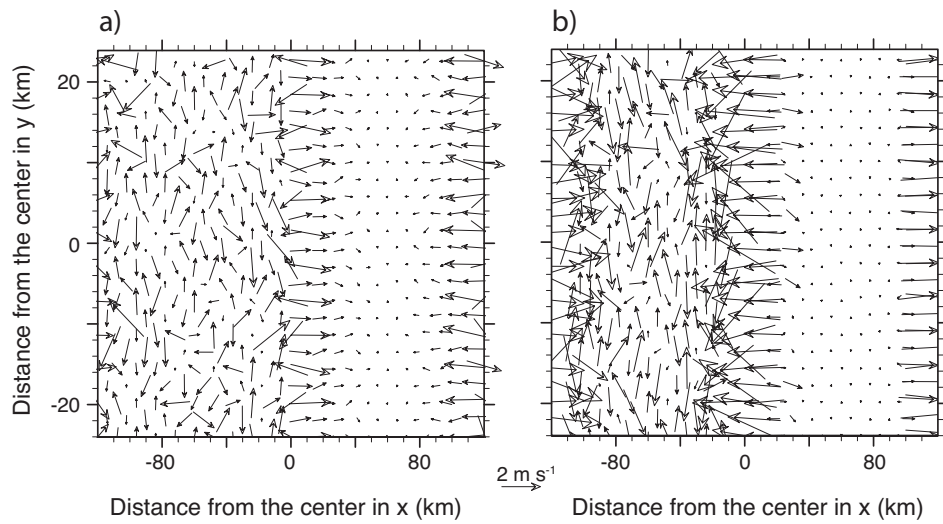
Fig. S3. x-y plot of the wind after (a) 3 and (b) 6 simulation hours. The perturbation in sensible heat flux is introduced after 2 h.
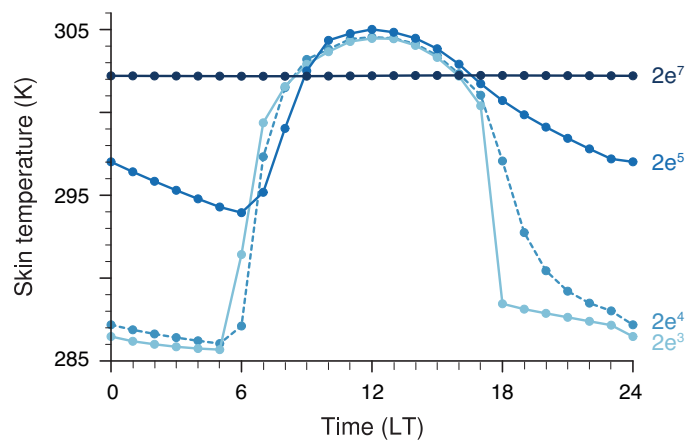
Fig. S4. Domain mean diurnal cycle of skin temperature on day 2 in simulations using different heat capacities, as indicated on the right-hand side of the curves (in J K^{-1} m^{-2}). The dashed line is for our standard configuration. Day 2 is chosen to avoid effects of the self-aggregation of convection on the diurnal cycle. Taking the mean only over the nonprecipitating area yields similar results.

Table S1. Simulation values needed to solve Eqs (1-4).

Eq. (1)	Q W m^{-2}	$F_{\text{SH}}(r_{\text{s}}=0)$ W m^{-2}	$\frac{\partial q_{\text{s}}}{\partial T}$ kg kg^{-1} K^{-1}	q_{s} kg kg^{-1}	RH -	r_{a} s m^{-1}
	380	37.9	0.0015	0.025	0.85	47

Eqs. (2-4)	θ_{v}^0 K	Γ K km^{-1}	t h	k -	H m
	297	4.5	12	0.37	1000

References

1. Betts AK (200) Idealized model for equilibrium boundary layer over land. *J. Hydrometeorol.*, **1**, 507-523.
2. Simpson JE (1969) A comparison between laboratory and atmospheric density currents. *Q J R Meteor Soc*, **95**, 758-765..
3. Seitter KL (1986) A numerical study of atmospheric density current motion including the effects of condensation. *J Atmos Sci*, **43**:3068-3076..
4. van Heerwaarden, CC (2011) Surface evaporation and water vapor transport in the convective boundary layer. *PhD thesis*, Wageningen University, 158pp., availabe at http://agris.fao.org/agris-search/search.do?recordID=NL2012006726..
5. Rieck M (2015) The role of heterogeneities and land-atmosphere interactions in the development of moist convection. *Bericht zur Erdsystemforschung*, **167**, 129pp, doi:10.17617/2.2095640..
6. Rochetin N, Lintner BR, Findell KL, Sobel AH, Gentine P (2014) Radiative-convective equilibrium over a land surface. *J Atmos Sci*, **27**:8611-8629..
7. Hohenegger C, Stevens B (2016) Coupled radiative convective equilibrium simulations with explicit and parameterized convection. *J Adv Model Earth Syst*, **8**:1468-1482..
8. Muller CJ, Held IM (2012) Detailed investigation of the self-aggregation of convection in cloud-resolving simulations. *J Atmos Sci*, **69**:2551-2565..
9. Becker T, Stevens B (2014) Climate and climate sensitivity to changing CO2 on an idealized land planet. *J Adv Model Earth Syst*, **6**:1205-1223..